Covalent Immobilization of Native Biomolecules onto Au(111) via *N*-Hydroxysuccinimide Ester Functionalized Self-Assembled Monolayers for Scanning Probe Microscopy

Peter Wagner, Martin Hegner, Peter Kernen, Frank Zaugg, and Giorgio Semenza
Department of Biochemistry, Swiss Federal Institute of Technology, ETH Zentrum, CH 8092 Zurich, Switzerland

ABSTRACT We have worked out a procedure for covalent binding of native biomacromolecules on flat gold surfaces for scanning probe microscopy in aqueous buffer solutions and for other nanotechnological applications, such as the direct measurement of interaction forces between immobilized macromolecules, of their elastomechanical properties, etc. It is based on the covalent immobilization of amino group-containing biomolecules (e.g., proteins, phospholipids) onto atomically flat gold surfaces via ω-functionalized self-assembled monolayers. We present the synthesis of the parent compound, dithio-bis(succinimidylundecanoate) (DSU), and a detailed study of the chemical and physical properties of the monolayer it forms spontaneously on Au(111). Scanning tunneling microscopy and atomic force microscopy (AFM) revealed a monolayer arrangement with the well-known depressions that are known to stem from an etch process during the self-assembly. The total density of the ω-*N*-hydroxysuccinimidyl groups on atomically flat gold was 585 pmol/cm^2, as determined by chemisorption of ^{14}C-labeled DSU. This corresponded to approximately 75% of the maximum density of the ω-unsubstituted alkanethiol. Measurements of the kinetics of monolayer formation showed a very fast initial phase, with total coverage within 30 s. A subsequent slower rearrangement of the chemisorbed molecules, as indicated by AFM, led to a decrease in the number of monolayer depressions in approximately 60 min. The rate of hydrolysis of the ω-*N*-hydroxysuccinimide groups at the monolayer/water interface was found to be very slow, even at moderately alkaline pH values. Furthermore, the binding of low-molecular-weight amines and of a model protein was investigated in detail.

INTRODUCTION

During the last dozen years a number of scanning probe microscopies (SPM) have established themselves as very powerful tools in surface and materials sciences. Their use with biological macromolecules and other biological objects, although spreading very rapidly, has not become routine yet. This is due to a number of factors, including the fragile nature of the biological materials, the limited resolution achieved so far as compared to that of high-resolution electron microscopy, and the need for specific preparation procedures (for reviews see Engel, 1991; Yang et al., 1993a; Hansma and Hoh, 1994; Lal and John, 1994; Morris, 1994; Bustamante et al., 1994; Shao and Yang, 1995).

In spite of their limitations, SPMs, in particular atomic force microscopy (AFM), are very attractive and promising techniques, because in principle they allow the study of biological objects under "physiological" conditions, i.e., in their native conformation, in aqueous buffers, in the presence of the appropriate ligands or effectors, etc. Ideally, biological objects should be firmly (covalently) immobilized to a smooth and inert substrate to avoid displacement by the tip (especially in the contact mode of operation) or removal from the surface (e.g., by injecting buffers in situ); this allows a broader choice of buffer conditions (ionic strength, ligand concentrations, pH) and modes of measurement (contact, tapping, non-contact, elasticity, adhesion, friction) to investigate biological objects. For example, electrostatic immobilization may set a limit to the ionic strengths in the buffer, or otherwise restrict the experimental conditions, i.e., when following in real time the dynamics of major structural changes. Although tapping mode AFM makes it easier to obtain stable images (but is often much more sensitive to sample contamination combined with less reproducible heights and lower lateral resolution) and considerably reduces a possible displacement of only loosely adsorbed biomolecules, it does not make covalent immobilization unnecessary. Especially when following dynamic processes by AFM in situ, it is often necessary to change the buffer in the fluid cell; only covalent-like attachment of the object to the substrate guarantees stable imaging. Furthermore, covalent anchoring of macromolecules to the substrate or to the tip is a must in some non-imaging applications, e.g., in the direct measurement of interaction forces between these macromolecules.

The most frequently used surfaces for reproducible and interpretable imaging of macromolecules in aqueous solutions include mica, with its excellent flatness (see, e.g., Yang et al., 1993b, 1994a,b; Schaper et al., 1994; Hansma

Received for publication 14 August 1995 and in final form 25 January 1996.

Dedicated to Prof. R. Hütter on the occasion of his retirement.

Address reprint requests to Dr. Giorgio Semenza and Dr. Peter Wagner, Department of Biochemistry II, ETH Zurich, Universitaetstrasse 16, CH-8092 Zurich, Switzerland. Tel.: 41-1-6323133; Fax: 41-1-6321089; E-mail: pwagner@cmgm.stanford.edu.

Dr. Wagner's present address is Department of Biochemistry, Stanford University School of Medicine, Beckman Center B407, Stanford, CA 94305-5307.

Dr. Hegner's present address is Institute of Physics, University of Basel, Klingelbergstrasse 82, CH-4056 Basel, Switzerland.

0006-3495/96/05/2052/15 $2.00

et al., 1993; Thundat et al., 1992; Lyubchenko et al., 1993; Guckenberger et al., 1994; Vesenka et al., 1993; Schabert and Engel, 1994; Kirby et al., 1995; Müller et al., 1995), and glass, which can be ω-functionalized via the reaction of organosilanes with the surface silanol groups (Plueddemann, 1991; Lyubchenko et al., 1993; Karrasch et al., 1993). Furthermore, HOPG (if used underivatized, but see Heckl et al., 1989, and Droz et al., 1994) binds macromolecules by way of weak electrostatic or "adsorption" forces (and, moreover, it has fallen into, perhaps excessive disrepute when it was shown to yield artifactual images mimicking DNA; Clemmer and Beebe, 1991; Heckl and Binnig, 1992).

Mica and glass have thus both proved their value in biological SPMs but suffer from two disadvantages: first, covalent attachment is either impossible or at least lengthy and less reproducible, and second, they are not suitable for applications requiring non-flat or patterned substrates, e.g., biosensor devices or AFM cantilevers.

The work presented in the following builds on our previous development of ultraflat Au(111) surfaces which having a mean roughness of 2–5 Å over areas larger than 25 μm^2 (Hegner et al., 1993; Wagner et al., 1995). It is also based on the profound and sophisticated knowledge of close-packed monolayers formed by alkanethiols and dialkyldisulfides on gold surfaces in a spontaneous self-assembly process (Nuzzo and Allara, 1983; Bain et al., 1989; Whitesides and Laibinis, 1990; Porter et al., 1987; Laibinis and Whitesides, 1992; Sellers et al., 1993). Such monolayers (if ω-functionalized, either ex situ or in situ) can provide organic interfaces with specific hydrophobicity and desired chemical reactivities at the liquid-monolayer interface, where the biomacromolecule is immobilized under "physiological" conditions, both for imaging and non-imaging investigations. This is also an essential prerequisite for the site-specific immobilization of proteins with respect to the substrate plane, something which is not possible by physisorption on mica.

In the following we describe the synthesis of dithio-bis(succinimidylundecanoate) (DSU, i.e., compound **4** in Scheme 1 and in Fig. 1) and the formation and the characteristics of self-assembled monolayers (SAMs) formed by it on ultraflat Au(111) surfaces, and report a few examples of its use in AFM imaging (see also Wagner et al., 1994). These SAMs of DSU are also being used successfully to measure directly the interaction forces between proteoglycans (Dammer et al., 1995) and between antigens and antibodies (Dammer et al., 1996).

MATERIALS AND METHODS

Materials

All chemicals were of highest available purity. Solvents were distilled before use or were of commercial grades of highest purity (Merck, Darmstadt, Germany). Ultrapure water with a resistance of 18 MΩ-cm was generally used for all aqueous buffers (purified by passage through a Barnstead Nanopure system). [1,4-^{14}C]Succinic anhydride was from ICN (Thame, England), and L-[U-^{14}C]lysine monohydrochloride (10.8 GBq/mmol; 293 mCi/mmol) was from Amersham Rahn (Zurich, Switzerland). [^{32}P]Sucrase isomaltase (EC 3.2.1.48-10) was prepared according to the method of Keller et al. (1995), with a specific activity of 22.1 GBq/mmol (597 mCi/mmol). Gold (99.99%) was purchased from Cendres and Metaux SA (Biel, Switzerland) and muscovite mica from Bal-Tec (Balzers, Liechtenstein). Monocrystalline Si(100) wafers were from Faselec (Zurich, Switzerland) and rinsed with chloroform before use. The epoxy glue epo-tek 377 was obtained from Polyscience (Zug, Switzerland).

General

^{1}H- and ^{13}C-NMR spectra were recorded on Bruker instruments (100 to 400 MHz). Chemical shifts (δ) are reported in parts per million relative to internal standard ($(CH_3)_4Si$, δ = 0.00 (^{1}H- and ^{13}C-NMR)). FAB mass spectra were recorded on a VG-SABSEQ instrument (Cs^+, 20 keV). Transmission infrared spectra were obtained as dispersions in KBr on a Fourier transform infrared spectroscopy (FTIR) Perkin-Elmer 1600 series instrument. Thin-layer chromatography (TLC) was performed on precoated silica gel 60 F254 plates (Merck), and detection was made using Cl_2/toluidine, $PdCl_2$, and UV detection under NH_3 vapor. Medium-pressure liquid chromatography was performed on a Labomatic MD-80 (Labomatic Instr. AG, Allschwil, Switzerland) using a Buechi column (460 × 36 mm; Buechi, Flawil, Switzerland) filled with silica gel 60 (particle size 15–40 μm) from Merck. All melting points (mps) are uncorrected.

Synthesis of 11,11′-dithio-bis(undecanoic acid) 3

Sodium thiosulfate (55.3 g, 350 mmol) was added to a suspension of 11-bromo-undecanoic acid **1** (92.8 g, 350 mmol) in 50% aqueous 1,4-dioxane (1000 ml). The mixture was heated at reflux (90°C) for 2 h until the reaction to the intermediate Bunte salt **2** was complete (clear solution). The oxidation to the corresponding disulfide was carried out in situ by adding iodine in portions until the solution retained a yellow to brown color. The surplus of iodine was retitrated with 15% sodium pyrosulfite in water. After removal of 1,4-dioxane by rotary evaporation the creamy suspension was filtered to yield product **3**. Recrystallization from ethyl acetate/tetrahydrofuran (THF) provided **3** as a white solid (73.4 g, 96.5%): mp 94°C; ^{1}H NMR (400 MHz, $CDCl_3/CD_3OD$ 95:5): δ 2.69 (t, 2H, J = 7.3 Hz), 2.29 (t, 2H, J = 7.5 Hz), 1.76–1.57 (m, 4H), and 1.40–1.29 (m, 12H); FAB-MS (Cs^+, 20 keV): *m/z* (relative intensity) 434 (100, M^+). Analysis calculated for $C_{22}H_{42}O_4S_2$: C, 60.79; H, 9.74; S, 14.75. Found: C, 60.95; H, 9.82; S, 14.74.

Synthesis of 11,11′-dithio-bis(succinimidylundecanoate) 4

To a solution of **3** (1.0 g, 2.3 mmol) in THF (50 ml) was added *N*-hydroxysuccinimide (HOSu, **5**; 0.575 g, 5 mmol) followed by dicyclohexylcarbodiimide (DCC) (1.03 g, 5 mmol) at 0°C. After the reaction mixture was allowed to warm to 23°C and was stirred for 36 h at room temperature, the dicyclohexylurea (DCU) was filtered. Removal of the solvent under reduced pressure and recrystallization from acetone/hexane provided **4** as a white solid. Final purification was achieved by medium-pressure liquid chromatography (9 bar) using silica gel and a 2:1 mixture of ethyl acetate and hexane. The organic phase was concentrated and dried in vacuum to yield **4** (1.12 g, 78%): mp 95°C; ^{1}H NMR (400 MHz, $CDCl_3$): δ 2.83 (s, 4H), 2.68 (t, 2H, J = 7.3 Hz), 2.60 (t, 2H, J = 7.5 Hz), 1.78–1.63 (m, 4H), and 1.43–1.29 (m, 12H); FAB-MS (Cs^+, 20 keV): *m/z* (relative intensity) 514 (100), 628 (86, M^+). Analysis calculated for $C_{30}H_{48}N_2O_8S_2$: C, 57.30; H, 7.69; N, 4.45; S, 10.20. Found: C, 57.32; H, 7.60; N, 4.39; S, 10.25.

Synthesis of *N*-hydroxy-[1,4-^{14}C]-succinimide [1,4-^{14}C]-5

[1,4-^{14}C]Succinic anhydride ([**1,4-^{14}C]-6**, 2.29 mg, 22.9 μmol, 250 μCi, specific activity 10.9 mCi/mmol, 403 MBq/mmol) was added to succinic anhydride (200.2 mg, 2 mmol) to adjust to a specific activity of 0.124 mCi/mmol. This mixture was added to a solution of hydroxylamine hydrochloride (139 mg, 2 mmol) and sodium hydroxide (80 mg, 2 mmol) in 14% aqueous 1,4-dioxane at a maximum temperature of 10°C. After stirring at 10°C for 1 h and at reflux (100°C) for 3 h, the solvents were completely removed by rotary evaporation, and the residue was extracted with boiling ethyl acetate (20 × 10 ml). The pooled organic phases were evaporated under reduced pressure and washed twice with diethylether. Drying in vacuum gave **[1,4-^{14}C]-5** as a TLC pure white solid (153.9 mg, 66%) (mp 91–93°C), which was used without further characterization for the synthesis of **[1,4-^{14}C]-4**.

Synthesis of 11,11′-dithio-bis([1,4-^{14}C]-succinimidylundecanoate)[1,4-^{14}C]-4

To a solution of **3** (264.7 mg, 0.61 mmol) in 5 ml THF, **[1,4-^{14}C]-5** (153.9 mg, 1.34 mmol) and DCC (275 mg, 1.34 mmol) were added at 0°C. After stirring for 24 h, the dicyclohexylurea was filtered and the solvent was removed by rotary evaporation. Recrystallization from acetone/hexane and liquid chromatography on 10 g silica gel 60 (particle size 40–63 μm) using ethylacetate/hexane (2:1) provided **[1,4-^{14}C]-4** as a white solid (119 mg, 31%; mp 95°C; NMR spectra were identical to those of **4**); TLC analyses gave single spots with R_f = 0.2 in ethylacetate/hexane (1:1). TLC detections were performed using the above-mentioned reagents and by visualization with PhosphorImaging. The specific activity of **[1,4-^{14}C]-4** was determined by scintillation counting to 0.24 mCi/mmol (8.9 GBq/mmol).

Preparation of ultraflat gold

These surfaces (mean roughness of 0.2–0.5 nm over 25 μm^2) were prepared as described elsewhere (Hegner et al., 1993; Wagner et al., 1995). In essence, gold was evaporated onto mica and glued upside down to a silicon wafer or glass coverslip; the mica was then removed by soaking in tetrahydrofuran. These "template-stripped" gold surfaces (TSG) consisted, therefore, of the gold atom layer that had been deposited on the mica template first.

Formation of DSU-SAM

Monolayers of **4** were prepared on TSG surfaces by immersing them in a solution of 11,11′-dithio-bis(succinimidylundecanoate) (DSU, **4**) in (freshly distilled) 1,4-dioxane at room temperature for varying periods of time and at different concentrations (see under Results). After rinsing with 5–7 ml 1,4-dioxane, the *N*-hydroxysuccinimidyl (NHS)-terminated monolayers were dried under a stream of nitrogen and immediately used for analysis and immobilization of lysine and sucrase-isomaltase, respectively.

Contact angle measurements

Contact angle goniometry was carried out on a G-I contact angle meter (Krüss, Hamburg, Germany) by applying a 3-μl drop of ultrapure water to a freshly prepared monolayer surface. A second drop of 3 μl was centered on the first, and the advancing contact angle was determined within 30 s. A set of ten locations was averaged per monolayer sample. The kinetics of hydrolysis has been determined by preparing SAM-**4** as a 1 mM solution of DSU in 1,4-dioxane for 1 h at room temperature. After rinsing with solvent, the monolayer samples were incubated in the appropriate aqueous solutions (phosphate buffer, pH 7.5 and 8.5, and 5 N NaOH, respectively) for the desired time and with THF rinsing before contact angle determination. The measurement of the kinetics of formation was achieved by immersing nine gold samples in solutions of DSU in 1,4-dioxane for varying times. After rinsing with solvent, the contact angles were determined by averaging ten readings on different locations of each surface.

Ellipsometry measurements

A Plasmos SD 2300 ellipsometer (Polyscience) was used for monolayer thickness measurements using a 70° angle of incidence with a ~1-mm-diameter beam at 623.8 nm (He-Ne laser). Samples were prepared by covering 50% of the gold platelet in a 1 mM solution of DSU in THF for various times (see kinetics of monolayer formation). For each data value three gold samples were measured in six sets of 30 locations oriented on a straight track ranging from the bare gold surface toward the SAM-covered surface. A refractive index of n = 1.50 was assumed, corresponding to an error of Δn = 0.05 and ±1.5–2 Å thickness.

Infrared measurements

Reflection absorption infrared spectra (RAIR) of SAMs were performed on a Nicolet 5 SXC FTIR spectrometer equipped with a liquid-nitrogen-cooled $Hg_xCd_{1-x}Te$-(MCT) detector. The reflection of the incident beam was carried out at an angle of incidence at 81°. Typically 400 scans at 4-cm^{-1} resolution were collected with an alternate slid-mediated calibration on a gold reference each 50 scans. The preparation of hydrolyzed SAM-4 (Fig. 5 *B*) has been carried out by incubation of the formerly measured monolayer for 30 min in a solution of 5 N NaOH, followed by extensive rinsing with solvents in the following order: H_2O, 1 N HCl, H_2O, and THF. The formation of SAM-**3** was achieved by immersing the gold samples in a 1 mM solution of **3** in THF for 1 h.

Atomic force microscopy

AFM was carried out on a NanoScope III from Digital Instruments (Santa Barbara, CA) equipped with different scanners with maximum scan ranges reaching from 0.7 to 140 μm. Microfabricated monocrystalline silicon tips (Lot, Darmstadt, Germany) with force constants ranging from 0.06 to 0.17 N/m were used. All images were taken under solution in a fluid cell and are based on unfiltered data. The measurement of the kinetics of monolayer formation was performed by immersing a freshly prepared TSG sample per time value in a 1 mM solution of DSU in 1,4-dioxane, followed by extensive rinsing with 1,4-dioxane.

Scanning tunneling microscopy

Scanning tunneling microscopy (STM) was carried out either on a Nanoscope III from Digital Instruments (with a modified STM tip-view head for a high tunneling resistance limit of 100 GΩ), or on a home-built STM with a maximum tunneling resistance of 10 TΩ. In both cases, mechanically cut PtIr tips (80/20) were used for measurements of ultraflat gold surfaces and monolayers.

Analysis of radiolabeling of SAM-4

The amount of chemisorbed DSU and the kinetics of film formation were monitored using ^{14}C-labeled DSU (**[1,4-^{14}C]-4**). Quantification of each sample has been done by two methods: i) digital imaging of radiolabeled SAMs, produced with a PhosphorImager scanner and quantified using internal standards and Imagequant 3.2 software (Molecular Dynamics, Sunnyvale, CA), and ii) total hydrolysis of the monolayer using 5 N NaOH and scintillation counting of the supernatant (Canberra Packard liquid scintillation counter CA 2400). Film formation and hydrolysis were carried out in a special multipurpose reaction chamber, which consists of 40 glass tubes; each of them was pressed with Kalrez O-rings (inner diameter 6.75 mm) onto 1-cm^2 TSG surfaces, thus enabling identical reaction conditions

(Wagner et al., 1995). Each of these chambers was loaded with TSG samples and filled with 1 ml of 1 mM DSU (**4**) in 1,4-dioxane. After the chosen time (30 s to 24 h), the supernatants were removed and the monolayer-covered gold samples were thoroughly rinsed 10 times with 1,4-dioxane (five ml each time). Fifty percent of the set (usually six gold samples per measured time) was air-dried and subjected to PhosphorImaging; the other half was immediately hydrolyzed with 1 ml of 5 N NaOH for 2 h, and the liberated amount of **[1,4-^{14}C]-5** was determined by liquid scintillation counting. The solutions used for rinsing were concentrated by rotary evaporation and checked for radioactivity by low-level scintillation counting to rule out the pressure of physisorbed radioactive material during air drying to guarantee the quantitative determination of the total amount of hydrolyzed HOSu in the supernatant. Dilutions of **[1,4-^{14}C]-4**, from 20 cpm to 8000 cpm, were air-dried on gold samples and used as internal standards for PhosphorImaging. The accuracy of the dilutions was also checked by scintillation counting.

Immobilization of [^{14}C]-lysine

The dependence of immobilization on pH and reaction time was determined with [U-^{14}C]-L-lysine. A drop of 20 μl of a 1.1 mM solution of lysine (specific activity adjusted to 26.6 mCi/mmol) in 50 mM phosphate buffer (pH ranging from 6.5 to 8.5) was applied onto a 1-cm^2 sample of SAM-**4** and placed in a chamber with 100% humidity. After the appropriate time the samples were thoroughly rinsed (in 2 ml buffer, 10 times), air-dried, and subjected to PhosphorImaging. Quantification was carried out using air-dried standards of [U-^{14}C]-L-lysine on TSG surfaces.

Immobilization of [^{32}P]-sucrase isomaltase

The dependence of immobilization on concentration was determined with protein kinase A [^{32}P]-phosphorylated sucrase isomaltase (SI; EC 3.2.1.48-10) (Keller et al., 1995) by either of two ways: 50 μl of the appropriate concentration (1–100 μg/ml) in phosphate-buffered saline (pH 7.5) was applied to a 1-cm^2 sample of SAM-**4** either as a 7-mm droplet or on a piece of parafilm, with the sample placed upside down on it. The former method has the advantage that the protein is only in contact with monolayer and air, but it often suffers, because of the surface tension, from uneven distributions of the protein in the droplet, which results in round circles of increased bound protein at the edges of the droplet. The latter circumvents this problem and guarantees a homogeneous concentration. In this case one has to be sure that the biomolecule will not be affected by the hydrophobic parafilm. We recommend this method as a standard procedure for the immobilization of proteins.

In both cases, the immobilization was finished after 1 h at room temperature in a special hood with 100% humidity. The samples were thoroughly rinsed with phosphate-buffered saline, air-dried, and subjected to PhosphorImaging. The resulting activities were approximately 15,000-fold higher than the background. Internal standards were used by air-dried dilutes of [^{32}P]-SI on monolayer surfaces.

RESULTS

Monolayer formation

Scheme 1 outlines the synthesis of DSU (**4**). The dicarboxylic acid (**3**) used as the precursor substance was easily prepared from 11-bromoundecanoic acid (**1**) by the formation of the intermediate Bunte salt (**2**), which was subsequently oxidized by iodine to yield **3**. The succinimide ester (**4**) was ultimately obtained by the classical HOSu/DCC method.

As substrates for the formation of SAMs from DSU (compound **4**) and for all other biological SPM applications,

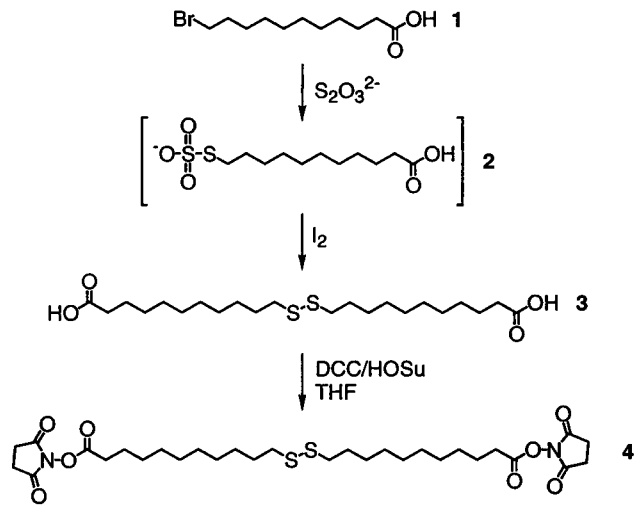

Scheme 1. Synthesis of dithio-bis(succinimidylundecanoate) (DSU; **4**)

we use ultraflat, template-stripped, polycrystalline Au(111) surfaces (TSGs), which had grown heteroepitaxially on mica. The remarkably small roughness of these "template-stripped" gold surfaces (typically 0.2–0.5 nm over 25 μm^2) is due to having made gold to grow onto atomically flat mica and using, after removal of the mica template, the very first atom layer of gold that had originally been deposited on the mica. The procedure for the removal of the mica template ("stripping") and the structural characterization of those TSG surfaces have been reported in detail elsewhere (Hegner et al., 1993; Wagner et al., 1995). A typical TSG surface is shown in the STM image of Fig. 2 *A*, taken at ambient conditions. Characteristic structural features are the completely annealed, atomically flat terraces (hundreds of nanometers in diameter), differing by only 3–5 atomic steps in *z*-height, and the triangular facets, which result from the (111) lattice. Atomic resolution STM images (data not shown) prove the heteroepitaxial nature of these Au(111) films, with the hexagonal (111) orientation and with lattice spacings of 0.288 nm and 0.499 nm for the nearest and the next-nearest neighbor distances, respectively.

An STM image of a monolayer formed by chemisorption of **4** onto these gold films is shown in Fig. 2 *B*, which was taken in the high-resistance range (0.6 TΩ) to avoid the destruction of the monolayer by the penetration of the tip. The structural topography of the SAM repeats that of the underlying gold surface in the shape and size of terraces separated by monoatomic steps and crossed by triangular facets. In addition, two black "holes" are visible, indicating discontinuities in the gold films (Fig. 2 *B*, *white arrows*). Smaller holes (Fig. 2 *B*, *black arrow*) are conspicuous constant structural features of self-assembled monolayers in SPM. These depressions are neither pinholes in the monolayer film nor SPM specific artefacts, but single-atom-deep etch pits resulting from an etching process during the chemisorption of the disulfide, i.e., they also are covered with **4**. Fig. 2 *B*, a contrast-enhanced STM image, shows evidence of these structural features of SAM-**4**. However,

when SAM-**4** is used as the immobilization carpet for biomacromolecules, the *z*-range is made to fit the height of the particular biological sample; this makes these tiny details of the monolayer disappear into the "background noise." The underlying SAM-Au surface thereby becomes totally featureless.

The kinetics of monolayer formation was examined by atomic force microscopy, ellipsometry, contact angle measurements, and radiolabeling. Fig. 2, *C–G*, shows an AFM study of 500 × 500 nm^2 areas of gold, immersed in a solution of **4** (1 mM, 1,4-dioxane) for various lengths of time, ranging from 1 s (Fig. 2 *C*) to 60 min (Fig. 2 *G*). Clearly, most of the surface is covered within 5 s. The "channels" that separate islands of monolayer regions are filled within seconds (Fig. 2, *C–E*), yielding an essentially continuous surface with only a few "holes." These holes disappear within 1 h (Fig. 2, *F–G*). It is important to note that the shape and number of these structures decrease with increasing time, i.e., they are indeed pinholes and not the etch pits mentioned above. The latter should increase with increasing immersion times and are due to a number of reasons less visible in the AFM images shown here compared to the STM image of Fig. 2 *B*. This very fast initial coverage was confirmed by contact angle and ellipsometrical measurements, as shown in Fig. 3, *A* and *B*. Both methods were used to follow the kinetics of monolayer formation at different concentrations of **4** in 1,4-dioxane. The monolayer thickness, estimated by ellipsometry (Fig. 3 *A*), depends on both concentration and time. A plateau of approximately 1.7 nm is reached in the minute time scale for a concentration of 1 mM, and 80–90% of this maximum value is obtained within 1 min. A concentration of 10 μM exhibits a more linear, slower increase in thickness and reaches 95% of the plateau only after 16 h, whereas with a 0.1 μM solution the plateau is not reached even after 1 week. The same kinetics are found from measurements of the advancing contact angles, $\theta_a(H_2O)$, which were determined after the spontaneous advance of the drop had come to a stop (Fig. 3 *B*). Because the monolayer surface is more hydrophilic than the bare gold surface, the $\theta_a(H_2O)$ values decrease with time. At 1 mM, the plateau of the isotherm is reached within 1 min, indicating that the contact angles are less sensitive to the density of the monolayer than is the ellipsometrical measurement. This can also be seen from the initial phase of the experiment at 0.1 μM, where the contact angle remains constant during the first minute, while the thickness exhibits 0.1 nm.

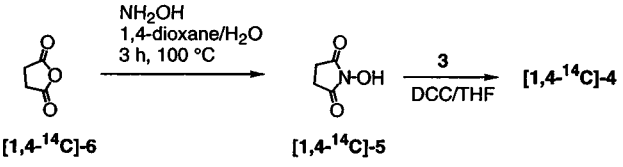

Scheme 2. Synthesis of ^{14}C-labeled dithio-bis(succinimidylundecanoate) (DSU; **[1,4-^{14}C]-4**).

A further possible method of examining the kinetics of monolayer formation is the use of radiolabeled compound **[1,4-^{14}C]-4** (synthesis outlined in Scheme 2). This would not only allow the determination of the kinetics of formation, but also the estimation of the concentration of molecules per surface area, which is an important parameter for describing the packing density of the monolayer. Furthermore, because the ^{14}C atoms are located in the leaving group, hydrolysis or reaction enables quantification of liberated radioactive material. Hence, quantification was carried out by two methods: i) digitalization using a PhosphorImager scanner and internal standards, and ii) total hydrolysis of the ω-*N*-hydroxysuccinimide from the monolayer and scintillation counting of the supernatant. Fig. 4 shows the kinetics of formation of the monolayer. Already within 30 s the plateau was reached at a level of 585 $pmol/cm^2$, which represented 75% of the theoretical value of a hexagonally close-packed, non-ω-functionalized alkanethiol. The plateau reached maintained its value during the observed time scale with a maximum of 24 h (see Fig. 4, *inset*). The dotted line in Fig. 4 refers to the data obtained from the liberated HOSu and agrees closely with those from PhosphorImaging.

To control the chemical functionality present on the surface, we performed a preliminary RAIR spectroscopy study of the SAM from DSU. Fig. 5 *A* shows the mid-IR region with the characteristic carbonyl absorption. After hydrolysis of the *N*-hydroxy-succinimidyl ester groups (by short incubation in 5 N NaOH) the C=O band disappears completely, although the carboxylic acid C=O functionality is still present (Fig. 5 *B*). This is probably due to conformational changes of the terminal headgroup (see also under Discussion). As a control, SAMs from the diacid (compound **3** in Scheme 1) showed RAIR spectra identical to those of hydrolyzed SAM (compare Fig. 5 *C* with Fig. 5 *B*).

Monolayer reactivity

Fig. 6 shows the kinetics of hydrolysis of SAMs from DSU under different conditions, as well as the reaction with ethylamine, as determined from the corresponding contact angles as a function of time ($\theta \approx 50°$, at $t = 0$). The reaction with ethylamine (20 mM in water, pH approximately 11) is characterized by two steps: the first leads to a hydrophobic, methyl group-terminated monolayer (a few hours), and the second leads to a slow increase in θ, not reaching a plateau even after 37.5 h. This increase shows that even at pH 11 the reaction with the amino groups is favored over hydrolysis. It is important to note that this experiment does not reflect the conditions to be fulfilled for protein immobilization for SPM applications, where full coverage is not desired for imaging individual anchored biomolecules.

Whereas the reaction with ethylamine leads to a more hydrophobic surface, hydrolysis at more or less alkaline pH values causes a significant increase in wettability (decrease of θ), the theoretical minimum of $\theta = 0°$ corresponding to

total hydrolysis (100% carboxylate surface). The kinetics of hydrolysis in phosphate buffers (pH 7.5 or 8.5) or in 5 N NaOH is shown in Fig. 6. As expected, in 5 N NaOH the contact angle drops sharply, and total hydrolysis is reached in approximately 2–3 h. This is in agreement with the determinations of liberated ^{14}C-labeled HOSu, which shows complete hydrolysis within 2 h under these conditions (see above). However, NHS squeezed in a monolayer arrangement was far more resistant to hydrolysis under neutral or moderately basic conditions than expected from data in solution: during the first 3 h at pH 7.5, hydrolysis is negligible, and even after 36 h at pH 7.5 or 8.5 the contact angles decrease by only about 10°.

The reactivity of SAM-**4** with amino acids was monitored by reacting with ^{14}C-labeled lysine. Fig. 7 *A* shows the pH dependence of lysine immobilization. A tenfold increase in reactivity was observed with increasing pH from 6.5 to 8.5. The amount of bound lysine was in the tens of picomoles per cm^2, which is approximately 5% of the binding sites theoretically available. The kinetics of lysine immobilization is shown in Fig. 7 *B*. As expected from Fig. 7 *A*, the slopes are steeper with increasing pH. It is important to note that no plateau was reached even after 20 h, indicating no saturation of the SAM.

The reaction of SAM-**4** with a model protein was studied using ^{32}P-labeled phosphorylated sucrase isomaltase (Fig. 8). This glycoprotein heterodimer was chosen because it can be phosphorylated by protein kinase A to a known extent (Keller et al., 1995), but it is otherwise an "average" protein, i.e., it is not particularly rich in lysine residues, it has a moderately acidic pI, etc. (Cogoli et al., 1972; Hunziker et al., 1986). The total amount of immobilized enzyme never exceeded 10 pmol/cm^2 (possibly because of the size of the protein, i.e., 260 kDa) and was a function of the protein concentration. At 1 μg/ml, which is a suitable concentration for SPM imaging, 23 ng enzyme was bound per cm^2, corresponding to 0.088 pmol/cm^2 or 5×10^{10} molecules/cm^2 or 500 molecules/μm^2. Fig. 8 also shows the binding efficiency, i.e., the ratio between immobilized protein and offered protein in the supernatant during the immobilization reaction. The resulting efficiency curve shows a maximum at the lowest concentration, then a steep decrease, followed by a slight increase, indicating two different kinetics (see also under Discussion).

DISCUSSION

Several questions concerning monolayer structure, kinetics of formation, stability, reactivity, interaction with SPM probes, and reproducibility must be addressed when working out a general immobilization procedure for biological samples. Many interfacial phenomena must be taken into account, like contaminations of the surface, interactions between topography and reactivity, effect of the atomically flat surface on reactivity, formation of charged surfaces, changes in the domain structure of the monolayer caused by the coupling procedure, reproducibility of the architecture of the anchored biomolecule, hydrophobicity, and (especially in SPM applications) interactions with the scanning tip and the risk of tip contamination from liberated leaving groups if immobilization is carried out in situ, etc. In a word, detailed studies with a variety of methods are necessary to understand the structure and behavior of these new organic systems.

The approach we have chosen, i.e., to use ω-functionalized monolayers on ultraflat gold surfaces, enables us not only to provide a reactive interface, but also to control the kind and degree of reactivity and hydrophobicity of these surfaces, and to overcome the serious problems of direct anchoring on bare gold. In addition, contaminants from the laboratory ambient or from compounds in the solutions adsorb onto gold within a short time. These adsorbates may affect the force interaction with the probing tip or cause tip contamination. These drawbacks are eliminated by self-assembled monolayers formed via thiol or disulfide chemisorption, because the high affinity of sulfur for gold leads to a self-cleaning effect. This is probably the reason why AFM imaging (also in solution) on monolayer-covered gold reveals a less contaminated gold topography than AFM on bare gold. Other advantages of using gold-directed monolayers include the possibility of constructing protein architectures on a nanometer scale (covalently bound to the substrate), which could be important, e.g., for biosensing devices. Furthermore, by choosing appropriate headgroups, other, more sophisticated immobilization strategies are possible in principle, such as reversible anchoring, site-specific immobilization, (e.g., Ni^{2+} chelators for binding polyhistidine fusion proteins; Wagner et al., manuscript in preparation), or multiple reactivities with switch-on activity. It is possible, e.g., to anchor a biomolecule first and to add appropriate ligands or effectors afterward (see Wagner et al., 1994).

Because the structural features of the gold surface show through the thin monolayer films, a minimal roughness of the substrate is essential. Template-stripped gold surfaces are exquisite supports toward this goal. The reader is referred to previous publications on this matter (Hegner et al., 1993; Wagner et al., 1995).

In contrast to the Langmuir-Blodgett technique, self-assembly of alkanethiol monolayers on Au(111) is a self-driven process and requires only the immersion of the gold platelet in a dilute solution of the thiol or disulfide. SAMs of non-ω-functionalized alkanethiols have been well characterized by SPM in different modes (e.g., Widrig et al., 1991; Kim and Bard, 1992; Alves et al., 1992; Liu and Salmeron, 1994; Poirier and Tarlov, 1994; Delamarche et al., 1994; Anselmetti et al., 1994; Wagner et al., 1995) and by a number of diffraction techniques (Strong and Whitesides, 1988; Chidsey et al., 1989; Chidsey and Loiacono, 1990; Samant et al., 1991; Fenter et al., 1993, 1994).

In contrast, the number of studies on ω-functionalized SAMs is far smaller, mainly for two reasons: i) functionalized alkanethiols are often not commercially available and

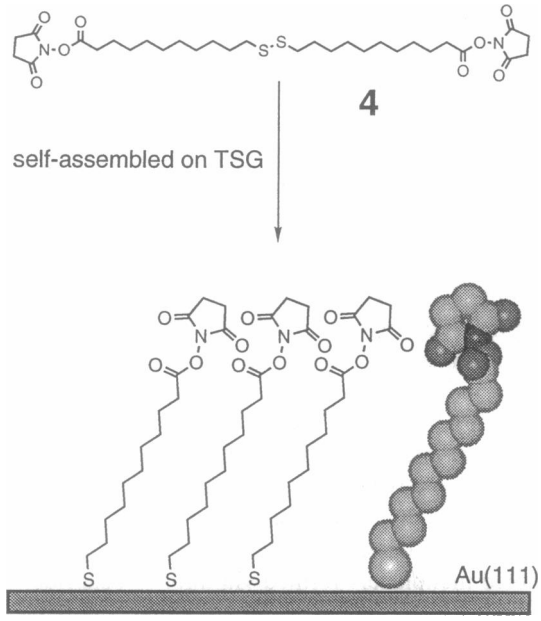

FIGURE 1 Self-assembled monolayer of DSU (4, in Scheme 1) on Au(111).

may be tricky to handle and purify, and ii) the introduction of even very small functionalities, e.g., amino groups, leads to additional difficulties in structural analyses (Sprik et al., 1994). In the example investigated in the present work, the bulky, large *N*-hydroxy-succinimidyl (NHS) group at the ω-position may interfere with a regular packing of the hydrocarbon chains of DSU (see Fig. 1). It is thus imperative to characterize these SAMs by a host of techniques; only a detailed analysis of the physical and chemical properties of this SAM allows us to exploit their potential in different kinds of SPM, such as imaging of dynamic events or force measurement of single molecule interactions.

Here we have investigated the following questions:

i. Does the chemisorption of DSU on Au(111) lead to a monolayer?

ii. How long does it take to reach (total) coverage?

iii. What is the density of molecules per surface area?

iv. Is the reactivity of the monolayer affected by the close packing?

v. What are the optimal conditions for achieving immobilization for SPM?

vi. Can monolayers from DSU be used in studies of biomolecules other than imaging?

(i) Formation of a monolayer from DSU on Au(111)

The nondestructive STM image carried out in the TΩ range as shown in Fig. 2B reveals the typical features of a monolayer, i.e., full coverage on completely annealed gold terraces and few hole-like depressions. It is important to emphasize that the holes and depressions seen in Fig. 2 *A* (bare gold) and Fig. 2 *B* (monolayer on gold) can have at least four different origins: i) very rare discontinuities in the gold film during deposition, which become apparent after stripping from the mica template as very deep holes (nanometer range) with diameters of 20 to 200 nm (shown in Fig. 2 *B* as *white arrows*); ii) small holes within atomically flat terraces of bare gold surfaces, exhibiting diameters of 3 to 6 nm and one atomic step deep, originating from incomplete coalescence during annealing in the deposition chamber (Fig. 2 *A*, *black arrow*). These depressions after formation of the monolayer are indistinguishable from the third group iii), which result from an etching process during the chemisorption of the disulfide compound (Sondag-Huethorst et al., 1994); they have the advantage of being strongly indicative of a monolayer, independently of ellipsometrical and wetting data. iv) Pinholes that are only apparent in the initial phase of monolayer formation, as shown in Fig. 2, *C–G*. None of these depressions, however, significantly alter the mean roughness.

(ii) Kinetics of formation of the SAM from DSU

The kinetics of film formation was studied by AFM imaging (Fig. 2, *C–G*), ellipsometry (Fig. 3 *A*), contact angle measurement (Fig. 3 *B*), and radiometry (Fig. 4). After a 1-s dipping in 1 mM DSU, approximately 50% of the gold surface (red channel-like areas) is already covered with adsorbate (yellow islands; Fig. 2 *C*). Within 25 s (Fig. 2 *E*) these islands coalesce, and the resulting pinholes decrease in number and size. The corresponding data from ^{14}C labeling indicate that within 30 s chemisorption is complete, i.e., it has reached a plateau without further increase. This very fast adsorption kinetics is remarkable for disulfides and even more for ω-functionalized ones such as DSU. After this initial phase, the adsorbed molecules rearrange, eliminating chain mismatches, which leads to a more densely packed arrangement. The corresponding AFM images in Fig. 2 *F* and Fig. 2 *G* describe this second phase, during which the very small depressions decrease further. This agrees also with ellipsometrical measurements (Fig. 3 *A*) and with the advancing contact angles of water (Fig. 3 *B*), which both show that it takes additional minutes for the plateau to be reached. In addition, the figures show a significant dependence on the concentration of DSU. At concentrations as small as 10 μM the plateau is reached after only 24 h. At 100 nM, which corresponds, given the total volume of solution, to exactly the same amount of DSU that can be adsorbed by a 1-cm^2 gold surface, the plateau is not reached even after 1 week. These findings also agree with the binding kinetics of alkanethiols, which showed a very fast initial phase, followed by a very slow rearrangement and increase in packing density, as measured by contact angles, ellipsometry, and second harmonic generation studies (Bain et al., 1989; Buck et al., 1991). One can conclude that for those applications where a tightly packed monolayer is desired, e.g., for structural studies of the SAM itself, or for SPM studies of small immobilized biomolecules, SAMs are best formed from DSU concentrations of 1 mM for 30 min, or of 10 μM for at least 24 h. However, in those applications for

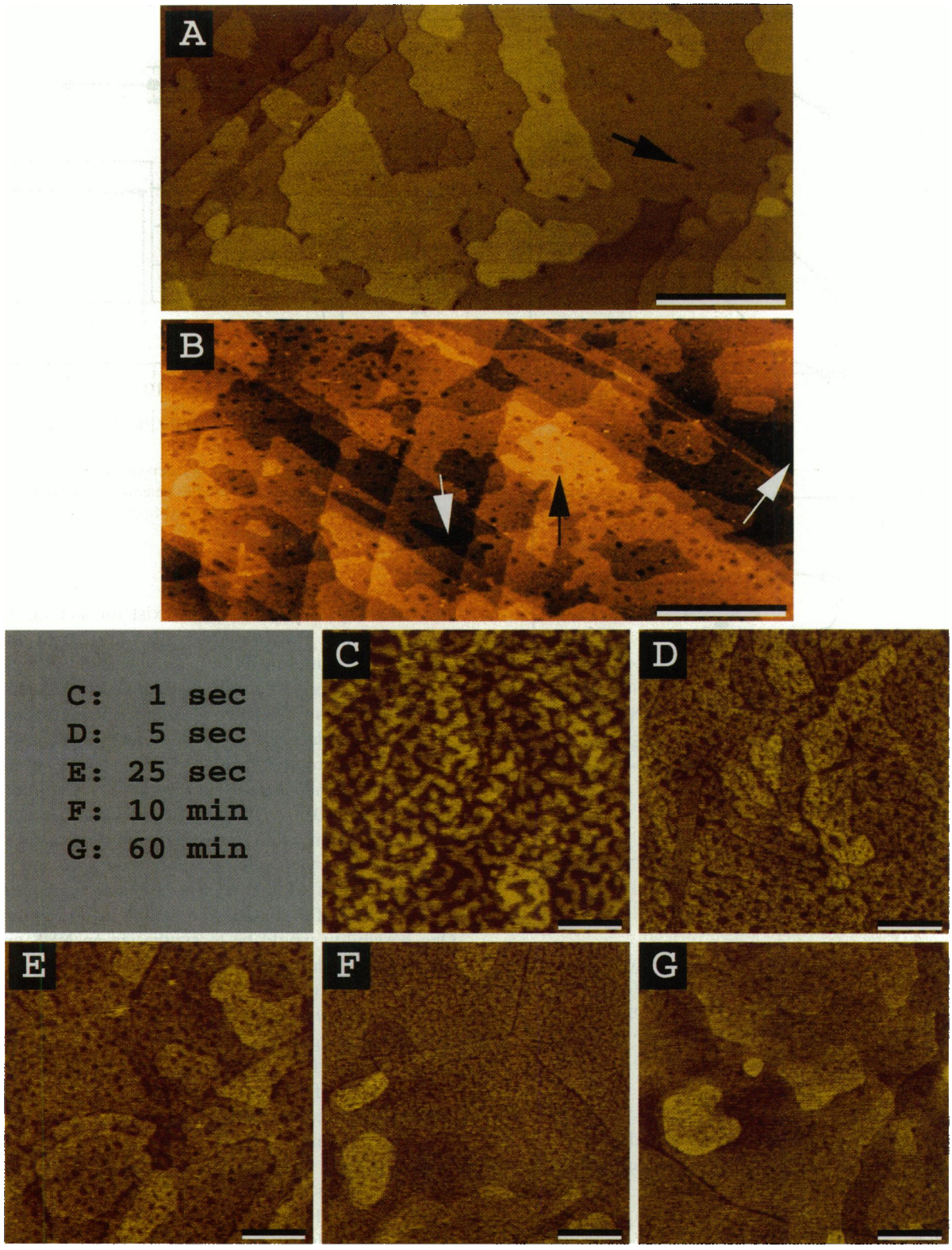

FIGURE 2 STM and AFM images of template-stripped gold surfaces (*A*) and of the SAM made from DSU (4, in Scheme 1) formed on them (*B–G*). Bars, 100 nm; z-range, 4 nm. (*A*) STM image (I_{tun} = 1 nA; U_{bias} = 200 mV) of a template-stripped gold (TSG) surface; the hole indicated by the black arrow is a one atom deep discontinuity within the atomically flat terrace. It results from incomplete coalescence during annealing. (*B*) STM image of SAM-4 on a TSG surface (I_{tun} = 2 pA; U_{bias} = 1.2 V). The hole indicated by a black arrow is a one atom deep depression resulting from an etch process during chemisorption. The holes indicated by the white arrows are the (rare) discontinuities in the gold film. (*C–G*) Kinetics of monolayer formation monitored by AFM on air-dried SAM-4. The times indicated refer to the lengths of immersion of TSG surfaces in 1 mM compound 4 in 1,4-dioxane (see text).

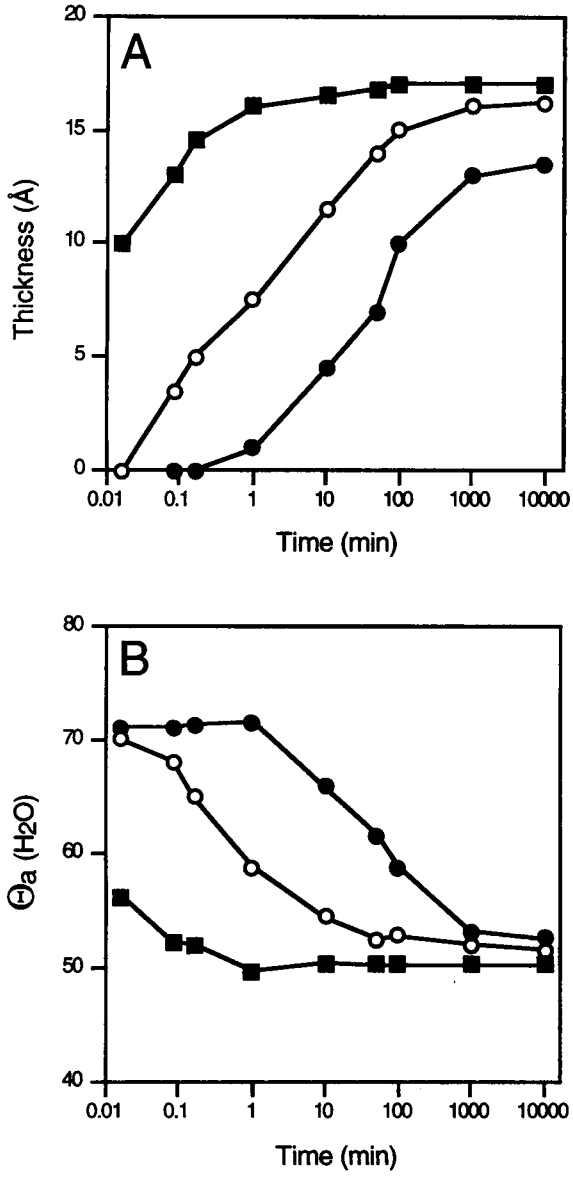

FIGURE 3 Kinetics of adsorption of dithio-bis(succinimidylundecanoate) 4 from 1,4-dioxane on ultraflat gold as a function of concentration: ■, 1 mM; ○, 10 μM; ●, 0.1 μM. (*A*) Thickness by ellipsometry. (*B*) Advancing contact angles (water). The standard errors are smaller than the symbols used.

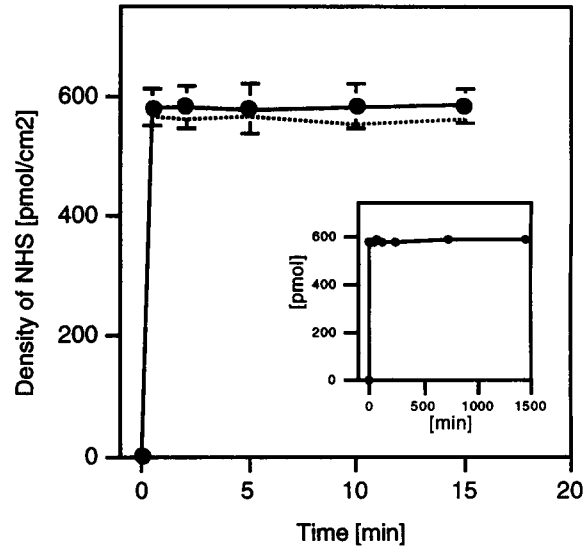

FIGURE 4 Kinetics of adsorption of compound [1,4-^{14}C]-4 (see Scheme 2) from 1,4-dioxane on ultraflat gold as determined by PhosphorImaging (●) and from [1,4-^{14}C]succinate liberated from [1,4-^{14}C]-4 by hydrolysis with 5 N NaOH for 2 h (*dotted lines*).

which the pinholes in Fig. 2 *A* are not detrimental (e.g., imaging with high *z*-range), dipping of the gold sample into a 1 mM solution for a few seconds should provide enough binding sites for immobilization. This makes the procedure of preparing a bioreactive surface a very fast and uncomplicated method.

(iii) Packing density of DSU on TSG surfaces

The total amount of chemisorbed molecules is an extremely important parameter for determination of the packing density of the monolayer, as well as for its binding efficiency and reactivity. Several methods exist for tackling this difficult question. The simplest way would be to count the molecules per area in those cases where STM yields molecular resolution. As mentioned above, this is not yet the case with SAMs from DSU. Neither the bicinchoninic acid/copper assay (data not shown; see also Tyllianakis et al., 1994) nor spectrophotometry or HPLC analyses of liberated HOSu showed adequate accuracy and sensitivity to quantitate adsorbed DSU. Attempts to calculate the density of DSU by reaction with ^{14}C-labeled amino acids suffer from nonquantitative yields due to steric hindrance and competitive hydrolysis of the NHS ester, and from unspecific physisorption of the radioactive amino acid onto the SAM. One possibility would be to synthesize an NHS analogon with an amino group at C-3 of the succinimidyl ring to have a labeling site, e.g., for [^{125}I]-Bolton-Hunter reagent, or a maleimido derivative for ^{35}S labeling. We have synthesized the former using Z-Asp as the starting compound, as previously reported (Aimoto and Richards, 1981). However, this method suffers from unpredictable reaction yields and from intermolecular quenching, if used on a SAM. Therefore, the best way, we think, is to introduce the radioactive nuclide into the leaving group of DSU itself, as outlined in Scheme 2. This enabled the quantitation of chemisorbed DSU, both by PhosphorImaging and from the amount of [1,4-^{14}C]-*N*-hydroxy-succinimide (compound **5** in Scheme 2) liberated upon reaction or hydrolysis. The results are shown in Fig. 4: the amount of NHS per square centimeter is 585 ± 20 pmol. This figure was obtained reproducibly in a number of experiments. The quantitation of solid-supported radioactive compounds by PhosphorImaging using internal standards has to be preferred to scintillation counting of the immersed solid material, because the counting

efficiency of the radionuclide bound to the gold surface is not known. The value of 585 pmol NHS residues/cm^2, which is 75% of the maximum packing density of nonfunctionalized alkanethiols (776 pmol/cm^2, assuming a tightly packed, hexagonal monolayer with a 5-Å chain separation and ($\sqrt{3} \times \sqrt{3}$)R30° overlayer structure), strongly suggests that the density of DSU on Au(111) is very high.

It is important to mention that the accuracy of these quantitations depends on the precise knowledge of the real surface area of the Au(111) substrate. Rough estimates may lead to serious errors, if accuracy in the tens of picomoles per square centimeter is required. However, in our studies the real surface area of the gold is nearly equivalent to the geometrical area, as described before. In addition, the preferential binding of sulfur to the threefold hollow sites of the Au(111) atom layer and the constriction by the hydrocarbon chains within the monolayer arrangement prevent adsorption on the sides of the terraces. Hence, the maximum number of adsorbed molecules is identical to the formal site density of the geometrical area.

(iv) Reactivity

We have carried out a grazing angle reflection absorption infrared spectroscopy study to obtain spectroscopical data from the chemical functionalities present on the monolayer. For SAM from DSU before (Fig. 5 *A*) and after (Fig. 5 *B*) hydrolysis, and (as a reference) SAM from the corresponding ω-carboxylate (compound **3** in Scheme 1; Fig. 5 *C*), spectra are shown in the mid-frequency 1850–1650 cm^{-1} regions. The bulk transmission spectrum of DSU in solution (not shown) exhibits four absorptions at 1820, 1788, 1744, and 1729 cm^{-1}, which must be assigned to the ester carbonyl, the in-phase, and the out-of-phase succinimidyl carbonyl groups. The reflection spectrum of its SAM shows a broader carbonyl band at ~1750 cm^{-1}, which is probably to be assigned to the two unresolved bands at lower frequency. The two absorptions at higher frequencies, which are weak in the transmission spectrum, are barely seen in the reflection spectrum as very weak protrusions. Moreover, these absorptions disappear completely if the succinimide group is removed by hydrolysis; the carboxylic acid carbonyl is still present. The resulting spectrum (Fig. 5 *B*) is identical to that of a SAM made from the diacid (compound **3** in Scheme 1) (Fig. 5 *C*) (the latter shows a C=O stretching band at 1696 cm^{-1} in the bulk transmission spectrum). These changes in the C=O absorptions from bulk to monolayer, and from DSU to the diacid, could be attributed to a broadening, indicating, e.g., hydrogen bonding, which makes them undetectable at our signal-to-noise ratios. Additionally, a further explanation might be the orientation of the transition dipole moments of the C=O groups with respect to the electric field of the light, i.e., those groups that are parallel to the surface exhibit no absorption. However, this would be rather unlikely, because previous studies on carboxylic acid SAMs showed distinct absorptions (Troughton et al., 1988; Duevel and Corn, 1992). Two other prominent bands of the C-O stretch appear in both the transmission and reflection spectra of DSU at 1210 and 1071 cm^{-1} (data not shown). A more detailed interpretation is beyond the scope of this work and will be the object of future studies. For example, it would be important to examine the high-frequency $\nu(CH_2)$ modes and the ratio between the band intensities of the C=O and CO-O modes. Furthermore, sharp progression bands in the 1345–1180 cm^{-1} region should be present if the hydrocarbon chains are in close arrangement, arising from interacting wagging vibrations of the $(CH_2)_x$ chains. In summary, one can conclude that the IR data confirm the existence of NHS groups in the monolayer and, furthermore, that hydrolysis in situ completely removes these groups (compare Fig. 5, *B* and *C*).

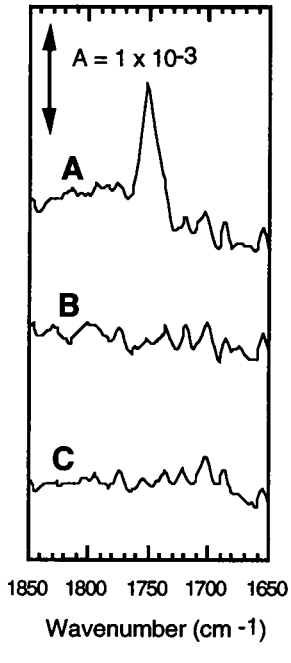

FIGURE 5 Mid-frequency region of a grazing angle FTIR (RAIR) spectrum of compound **4** chemisorbed as a monolayer on template-stripped gold before (*A*) and after (*B*) hydrolysis, and of SAM-**3** (*C*) (control).

As a further approach, we have determined the reactivity of the monolayer toward nucleophilic groups by contact angle measurement. Fig. 6 shows the time dependence of hydrolysis at different pHs and the reaction with ethylamine, determined by contact angle goniometry (starting value for $t = 0$: $\theta_a(H_2O) \approx 50°$). The progress of hydrolysis can be followed by the decrease in θ_a, because the resulting carboxylate headgroups are totally wettable by water, i.e., for complete hydrolysis a contact angle of $\theta_a(H_2O) = 0°$ can be expected. Hydrolysis of the NHS ester is very slow at pH 7.5 and 8.5 (100 mM phosphate buffer) and is not complete even after the maximum time allowed by this experiment (37.5 h). This is rather surprising, because the hydrolysis of NHS derivatives in solution has a half-life of 1 h at pH 8.0 (25°C) and 10 min at pH 8.6 (4°C) (Staros, 1988). One can assume that the monolayer arrangement decreases the

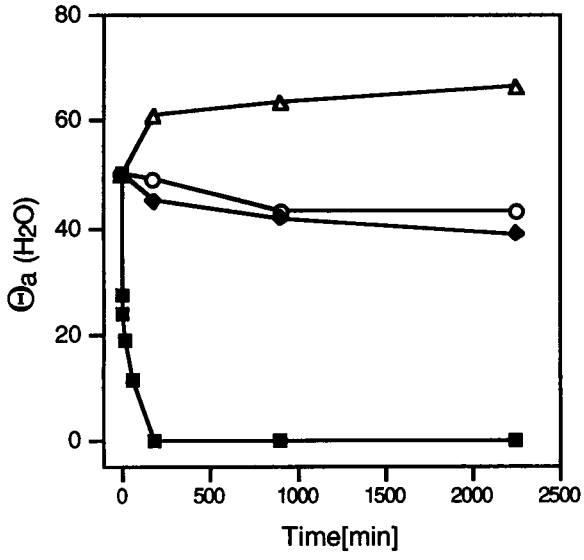

FIGURE 6 Kinetics of hydrolysis of chemisorbed DSU **4** as a SAM in alkaline milieu [5 N NaOH (■); 100 mM phosphate buffer, pH 8.5 (◆); 100 mM phosphate buffer, pH 7.5 (○)] and of the reaction of SAM-**4** with 20 mM ethylamine (△) at pH 11; both were determined from the advancing contact angle (water).

reactivity, possibly because of the orientation of the sp^2 carbon and/or the steric hindrance of the succinimidyl moieties. At any rate, there is no danger of hydrolysis, when biomolecules were immobilized at pH 7–8.5 over long periods of time. On the other hand, quenching of the binding sites by increasing the pH to 8.5 without amines after the immobilization of the biomolecule is inefficient. Only treatment with 5 N NaOH leads to a complete hydrolysis in 2–3 h by contact angle measurements (at this pH the succinimidyl also is cleaved, which, however, affects neither the results of contact angle measurement nor those of the radiometry, reported above). The contact angle of 0° after hydrolysis corresponds to the angle obtained on SAMs from the diacid (compound **3** in Scheme 1) (data not shown). Because the contact angles are sensitive toward the packing density of a monolayer, one could in principle draw the conclusion that the density of the molecules in SAM from DSU should be similar to that of a tightly packed monolayer of the corresponding diacid with its smaller headgroup functionality. However, interpretations of contact angles in the range of full wettability should be drawn with care, and we do not derive these conclusions only from contact angle determination. We have not yet examined the short-time kinetics of hydrolysis from the liberation of [1,4-^{14}C]-*N*-hydroxy-succinimide (compound **5** in Scheme 2). In the radiometrical kinetics measurement, hydrolysis was complete after 2 h, which is in agreement with the contact angle measurements shown in Fig. 6.

The reaction with ethylamine can be monitored by the increase in contact angle due to the appearance of hydrophobic methyl-group terminations on SAMs from DSU. Using a 20 mM ethylamine solution (pH 11.0), a fast initial increase in the first 3 h and a further moderate increase during the next 35 h was observed. This shows again that the kinetics of reaction of DSU as a monolayer is slower than in solution. NHS groups in compounds dissolved in water usually exhibit reaction times in the range of minutes; for example, the reaction of a short-chain homolog of DSU with an amine-derivatized glass surface is complete within 2 min (Lomant and Fairbanks, 1976). It is important to note that with SAMs from DSU, no plateau was reached, indicating enough binding capacity, even after 37.5 h at pH 11 (Fig. 6). Furthermore, at this pH and in the presence of moderate concentrations of amines, hydrolysis is negligible. However, this cannot be assumed if the target is present in very low concentrations, where hydrolysis is preferred, e.g., when proteins have to be immobilized in very low concentrations suitable for SPM imaging.

We have determined covalently immobilized biomolecules such as [^{14}C]lysine (Fig. 7, *A* and *B*) and [^{32}P]-sucrase-isomaltase (Fig. 8), after thorough removal of those that were merely physisorbed. Fig. 7 *A* shows the pH dependence of [^{14}C]lysine binding on SAM made from DSU and Fig. 7 *B* the kinetics of [^{14}C]lysine binding at pH 6.5, 7.5, and 8.5, respectively. The kinetics is faster at higher pH. This is not unexpected, because of the increased deprotonation of the amino groups. However, at high pH, the reason for the very fast reaction may be somewhat more complex, because at alkaline pH values SAMs from DSU are partly hydrolyzed to a very small extent (see contact angle measurements above); this may increase the accessibility for attacking the sp^2 carbons of neighboring non-hydrolyzed DSU molecules. This accelerated binding attributed to limited hydrolysis is also indicated by the fact that pretreatment of SAMs from DSU with buffer at pH 8.5 slightly increases the amount of protein bound (data not shown). Importantly, this provides a further indication of the tightly packed arrangement in the SAMs formed by DSU.

Furthermore, the total amount of bound [^{14}C]lysine is only approximately 2–5% of the maximum binding site density of 585 pmol/cm^2, even after approximately 35 h, with large residual binding capacity still present (no plateau was reached). This binding efficiency may seem small when compared with that of porous materials but is, in fact, very high for the immobilization of proteins for SPM imaging of individually anchored biomolecules, where approximately 5×10^8 molecules (8.3 attomoles/cm^2) is desired. SAMs from DSU bind this amount at protein concentrations as low as 10–1000 ng/ml. The combined high capacity and slow kinetics of the reaction make it easy to control the amount of immobilized biomolecules and to immobilize very rare biomolecules.

(v) Conditions for binding proteins to SAMs of DSU for SPM imaging

This very high binding efficiency toward very dilute protein solutions can also be seen in Fig. 8, showing the immobilization of phosphorylated sucrase isomaltase. The total

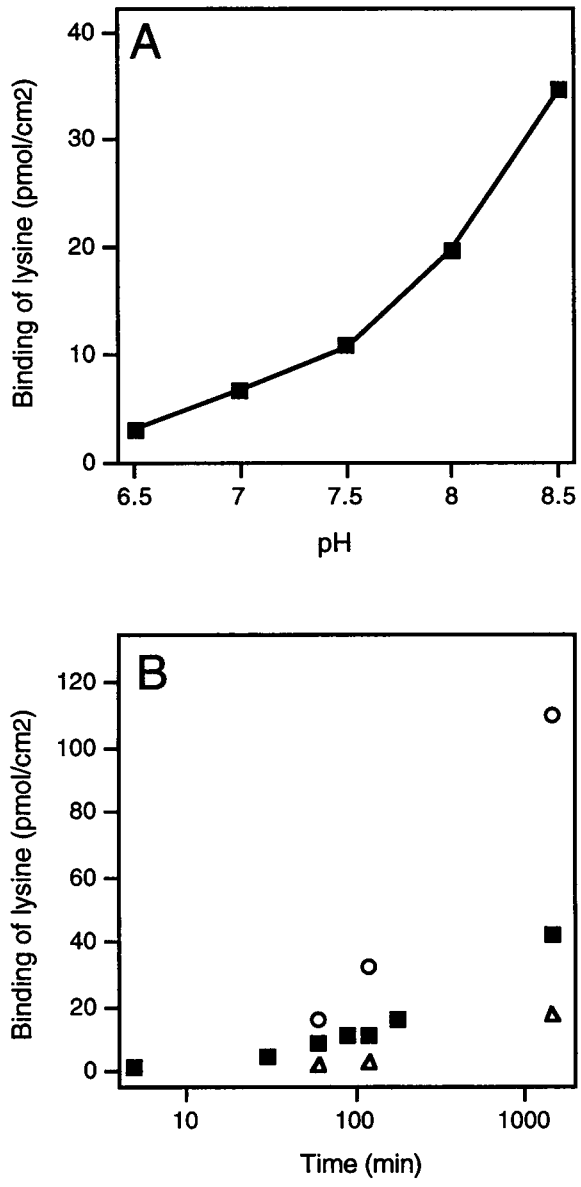

FIGURE 7 Binding of [^{14}C]-L-lysine by a self-assembled monolayer of dithio-bis(succinimidylundecanoate) 4. (*A*) pH dependence. (*B*) Time course. △, pH 6.5; ■, pH 7.5; ○, pH 8.5.

amount of bound protein increases with increasing concentration, but the binding efficiency, i.e., the ratio of immobilized protein to offered protein in the droplet, has its maximum at the lowest concentration of 1 μg/ml (45% of the total offered amount of sucrase isomaltase (50 ng) has been immobilized). The decrease and then the rise in the efficiency curve with increasing concentrations make it likely that at very low concentrations the process is diffusion controlled, i.e., all molecules coming in close contact with the bioreactive surface are bound. These experiments also show the absence of a plateau at higher concentrations of 100 μg/ml, indicating a persistent binding capacity over long periods of time (hours).

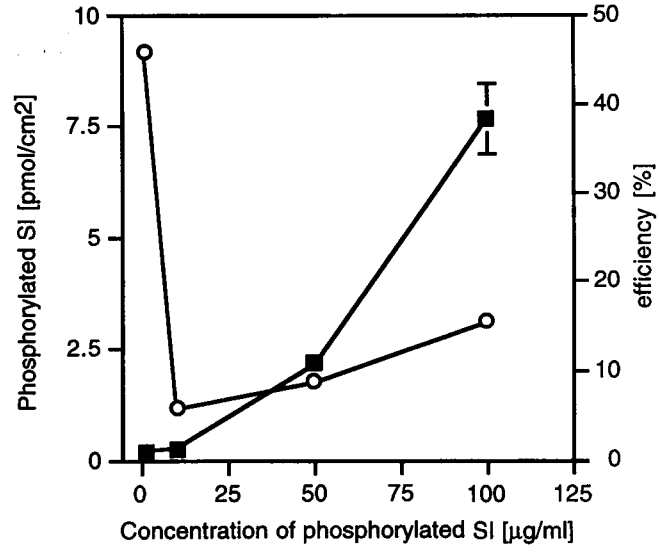

FIGURE 8 Concentration-dependent binding of [^{32}P]-sucrase-isomaltase. ■, total amount; ○, efficiency.

We have not yet investigated systematically the reaction of SAMs from DSU with different nucleophilic targets and in different kinds of buffers. However, one can expect the highest reactivity toward primary amines, i.e., lysine residues and N-terminal amino groups in proteins, or phosphatidylethanolamine in phospholipids. Introducing additional amino groups can make any biomolecule accessible to this method. A wide range of buffer systems is compatible with immobilization on this SAM, but amino group-containing buffers, e.g., Tris or glycine buffers, should of course be avoided.

(vi) Final considerations: imaging and non-imaging SPM based on SAMs from DSU on TSG surfaces

The results obtained from radiometry, SPM, and kinetics reported in this study demonstrate a densely packed monolayer arrangement of DSU molecules on the TSG surface. We can outline a standard protocol for SPM applications as follows. The SAM should be formed by immersion of a gold platelet (preferably TSG; see Hegner et al., 1993; Wagner et al., 1995) in 1 mM DSU in 1,4-dioxane for 30 min at room temperature. After rinsing, immobilization of proteins should be carried out at concentrations of 10–1000 ng/ml and at pHs between 7.5 and 8.5 (amine-free buffers) for 10–60 min. Lower pH values are also possible, because we have successfully immobilized clathrin cages at pH 6.5 within 1 h (Wagner et al., 1994).

Fig. 9 shows a few selected examples of different biomolecules, such as collagen V (Fig. 9, *A* and *G*), clathrin (Fig. 9, *B* and *C*), DNA fragments (Fig. 9 *D*), and liposomes (Fig. 9 *E*). All of them were immobilized on SAMs made from DSU and imaged under native conditions, which is a necessary prerequisite for investigating biochemical, dynamic-related, or force-

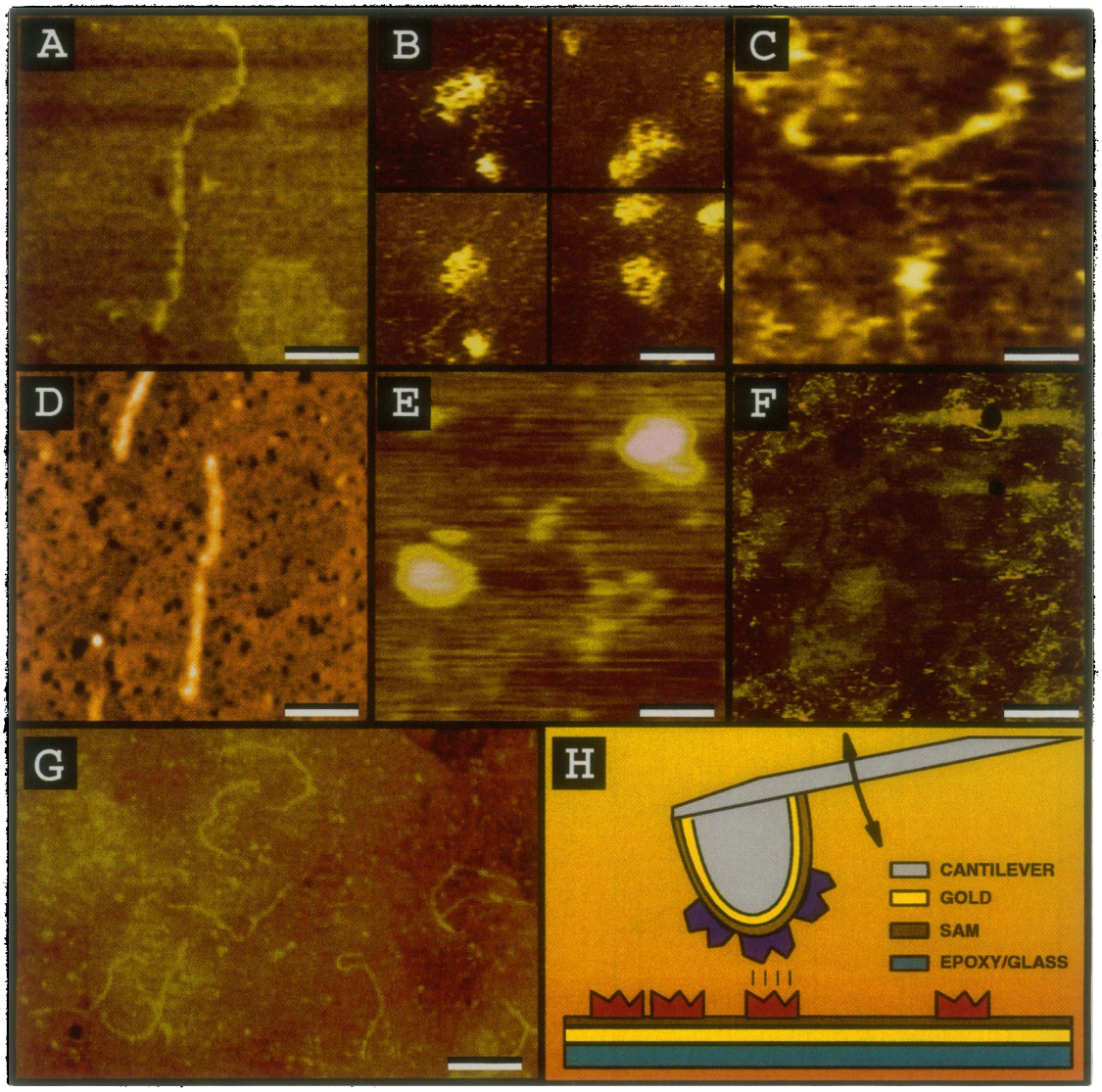

FIGURE 9 AFM images of selected native biomolecules covalently immobilized on a self-assembled monolayer of dithio-bis(succinimidylundecanoate) (DSU, compound **4**) and investigated in appropriate amine-free buffer solutions. (*A*) Collagen V single molecule (contour length 300 nm) immobilized in phosphate buffer (pH 7.0) at a concentration of 25 ng/ml (for details see Zaugg et al., manuscript in preparation; see also *G*). Bar, 70 nm; z-range, 5 nm. (*B*) Clathrin "baskets" during in situ disassembly (from Wagner et al., 1994). Bar, 470 nm. (*C*) Clathrin triskelion from the same experiment as in *B*. Bar, 20 nm. (*D*) Amino-modified DNA fragment (contour length 220 nm), tapping mode. Bar, 50 nm; z-range, 8 nm (for details see Hegner et al., 1996). (*E*) Liposomes (phosphatidylcholine:phosphatidylethanolamine, 80:20). Bar, 400 nm; z-range, 50 nm (for details see Kernen et al., manuscript in preparation). (*F*) Triskelia physisorbed on hydrolyzed SAM-4 (thus carrying ω-carboxylate groups only). The central part of this image is free of triskelia because multiple scans have wiped away the loosely bound triskelia. This demonstrates the importance of stable, covalent immobilization (compare with *B* and *C*). Zooming out showed, only in the first scan, biological material lying in the surrounding area, which was not resolved satisfactorily. Bar, 330 nm; z-range, 8 nm. (*G*) Collagen V single molecules immobilized onto SAMs from DSU as described in *B* but imaged by tapping mode. Bar, 150 nm; z-range, 5 nm. (*H*) Schematic view of the experimental set-up for measuring interaction forces. Two different biomolecules (*red* and *dark blue*) were covalently bound to Au(111) via SAMs from DSU to the tip and to the substrate, respectively (e.g., for biotinylated serum albumin and anti-biotin antibodies, see Dammer et al., 1996, and for proteoglycans, see Dammer et al., 1995).

related questions on the very same samples. In contrast, Fig. 9 *F* is an example of noncovalent physisorption leading to insufficient immobilization and, therefore, unsuccessful AFM imaging (for details, see Fig. 9 legend). These figures show that our method can be successfully used for covalently immobilizing and imaging proteins, nucleic acids, and phospholipids under native conditions. Our approach allows experimental set-ups that are impossible on mica or glass. In situ observation by SPM of dynamic processes of covalently immobilized biomolecules is possible, e.g., by the exchange of the medium (change of ligand concentration, ionic strength, pH, etc.). Pressure gradients and perturbations during injection of reactants or buffers may rinse away (loosely) physisorbed biological material.

In a further approach we have coated the AFM cantilever with a thin layer of gold followed by chemisorption of a

monolayer, revealing an organic interface at the very end of the tip. An application is, for example, the use of hydrophobic alkanethiol monolayers to achieve better resolution by reducing the interactions with the hydrophilic sample.

A more sophisticated application of DSU-coated Au cantilevers is their use in the direct measurement of the interaction forces between proteoglycans (Dammer et al., 1995) or between antigen and antibody (Dammer et al., 1996) (see Fig. 9 *H* for a schematic view). Clearly, SPMs in the imaging mode are not the only areas in which SAMs from DSU can advantageously be used to anchor biological macromolecules to a Au(111) support.

In general, these self-assembled monolayers of appropriately ω-functionalized alkanethiols on ultraflat Au(111) surfaces provide tools in a number of nanotechnological applications, because of the ease with which organic interfaces of different desired reactivities and other properties can be prepared.

We are grateful to Profs. H.-J. Güntherodt and U. Suter for their support. We thank Drs. W. Caseri and M. Schirle for their help with reflection absorption infrared spectroscopy, Dr. P. Keller for providing us with phosphorylated sucrase isomaltase, Th. Maeder for helpful discussions, and A. Lehmann for technical assistance. Thanks are also due to Prof. H. Hauser for critical reading of the manuscript and helpful comments.

This work was supported in part by grants from the ETH Zurich, Ciba-Geigy Jubiläums-Stiftung Basel, the Schweizerische Krebsliga, and the Schweizerische Reinraumgesellschaft.

REFERENCES

Aimoto, S., and F. M. Richards. 1981. Synthesis of carriers of differing stokes radius with activated acyl groups for use as reagents in labeling membrane proteins. *J. Biol. Chem.* 256:5134–5143.

Alves, C. A., E. L. Smith, and M. D. Porter. 1992. Atomic scale imaging of alkanethiolate monolayers at gold surfaces with atomic force microscopy. *J. Am. Chem. Soc.* 114:1222–1227.

Anselmetti, D., A. Baratoff, H.-J. Güntherodt, E. Delamarche, B. Michel, Ch. Gerber, H. Kang, H. Wolf, and H. Ringsdorf. 1994. Domain and molecular superlattice structure of dodecanethiol self-assembled on Au(111). *Europhys. Lett.* 27:365–370.

Bain, C. D., E. B Troughton, Y.-T. Tao, J. Evall, G. M. Whitesides, and R. G. Nuzzo. 1989. Formation of monolayer films by the spontaneous assembly of organic thiols from solution onto gold. *J. Am. Chem. Soc.* 111:321–335.

Buck, M., F. Eisert, J. Fischer, M. Grunze, and F. Träger. 1991. Investigation of self-organizing thiol films by optical second harmonic generation and x-ray photoelectron spectroscopy. *Appl. Phys. A.* 53:552–556.

Bustamante, C., D. A. Erie, and D. Keller. 1994. Biochemical and structural applications of scanning force microscopy. *Curr. Opin. Struct. Biol.* 23:115–139.

Chidsey, C. E. D., G.-Y. Liu, P. Rowntree, and G. Scoles. 1989. Molecular order at the surface of an organic monolayer studied by low energy helium diffraction. *J. Chem. Phys.* 91:4421–4423.

Chidsey, C. E. D., and D. N. Loiacono. 1990. Chemical functionality in self-assembled monolayers: structural and electrochemical properties. *Langmuir.* 6:682–691.

Clemmer, C. R., and T. P. Beebe, Jr. 1991. Graphite: a mimic for DNA and other biomolecules in scanning tunneling microscope studies. *Science.* 251:640–642.

Cogoli, A., H. Mosimann, C. Vock, A. K. v. Balthazar, and G. Semenza. 1972. A simplified procedure for the isolation of the sucrase-isomaltase complex from rabbit intestine. Its amino acid and sugar composition. *Eur. J. Biochem.* 30:7–14.

Dammer, U., M. Hegner, D. Anselmetti, P. Wagner, M. Dreier, W. Huber, and H.-J. Güntherodt. 1996. Specific antigen/antibody interactions measured by force microscopy. *Biophys. J.* 70:In press.

Dammer, U., O. Popescu, P. Wagner, D. Anselmetti, H.-J. Güntherodt, and G. N. Misevic. 1995. Quantification of the intermolecular binding strength for a cell adhesion proteoglycan by scanning force microscopy. *Science.* 267:1173–1175.

Delamarche, E., B. Michel, Ch. Gerber, D. Anselmetti, H.-J. Güntherodt, H. Wolf, and H. Ringsdorf. 1994. Real-space observation of nanoscale molecular domains in self-assembled monolayers. *Langmuir.* 10: 2869–2871.

Droz, E., M. Taborelli, P. Descouts, and T. N. C. Wells. 1994. Influence of surface and protein modification on immunoglobulin G adsorption observed by scanning force microscopy. *Biophys. J.* 67:1316–1323.

Duevel, R. V., and R. M. Corn. 1992. Amide and ester surface attachment reactions for alkanethiol monolayers at gold surfaces as studied by polarization modulation fourier transform infrared spectroscopy. *Anal. Chem.* 64:337–342.

Engel, A. 1991. Biological applications of scanning probe microscopies. *Annu. Rev. Biophys. Biophys. Chem.* 20:79–108.

Fenter, P., A. Eberhardt, and P. Eisenberger. 1994. Self-assembly of *n*-alkylthiols as disulfides on Au(111). *Science.* 266:1216–1218.

Fenter, P., P. Eisenberger, and K. S. Liang. 1993. Chain-length dependence of the structures and phases of $CH_3(CH_2)_n{}_{-1}SH$ self-assembled on Au(111). *Phys. Rev. Lett.* 70:2447–2450.

Guckenberger, R., M. Heim, G. Cevc, H. F. Knapp, W. Wiegräbe, and A. Hillebrand. 1994. Scanning tunneling microscopy of insulators and biological specimens based on lateral conductivity of ultrathin water films. *Science.* 266:1538–1540.

Hansma, H. G., M. Bezanilla, F. Zenhäusern, M. Adrian, and R. L. Sinsheimer. 1993. Atomic force microscopy of DNA in aqueous solutions. *Nucleic Acids Res.* 21:505–512.

Hansma, H. G., and J. H. Hoh. 1994. Biomolecular imaging with the atomic force microscope. *Annu. Rev. Biophys. Biomol. Struct.* 23: 115–139.

Heckl, W. M., and G. Binnig. 1992. Domain walls on graphite mimic DNA. *Ultramicroscopy.* 42–44:1073–1078.

Heckl, W. M., K. M. R. Kallury, M. Thompson, C. Gerber, H. J. K. Hörber, and G. Binnig. 1989. Characterization of a covalently bound phospholipid on a graphite substrate by x-ray photoelectron spectroscopy and scanning tunneling microscopy. *Langmuir.* 5:1433–1435.

Hegner, M., M. Dreier, P. Wagner, G. Semenza, and H.-J. Güntherodt. 1996. Modified DNA immobilized on bioreactive self-assembled monolayer on gold for dynamic force microscopy imaging in aqueous buffer solution. *J. Vac. Sci. Tech. B.* In press.

Hegner, M., P. Wagner, and G. Semenza. 1993. Ultralarge atomically flat template-stripped Au surfaces for scanning probe microscopy. *Surf. Sci.* 291:39–46.

Hunziker, W., M. Spiess, G. Semenza, and H. F. Lodish. 1986. The sucrase-isomaltase complex: primary structure, membrane orientation, and evolution of a stalked, intrinsic brush border protein. *Cell.* 46: 227–234

Karrasch, S., M. Dolder, F. Schabert, J. Ramsden, and A. Engel. 1993. Covalent binding of biological samples to solid supports for scanning probe microscopy in buffer solution. *Biophys. J.* 65:2437–2446.

Keller, P., G. Semenza, and S. Shaltiel. 1995. Phosphorylation of the N-terminal intracellular tail of sucrase-isomaltase by cAMP-dependent protein kinase. *FEBS Lett.* 233:963–968.

Kim, Y. T., and A. J. Bard. 1992. Imaging and etching of self-assembled *n*-octadecanethiol layers on gold with the scanning tunneling microscope. *Langmuir.* 8:1096–1102.

Kirby, A. R., A. P. Gunning, V. J. Morris, and M. J. Ridout. 1995. Observation of the helical structure of the bacterial polysaccharide acetan by atomic force microscopy. *Biophys. J.* 68:360–363.

Laibinis, P. E., and G. M. Whitesides. 1992. ω-Terminated alkanethiolate monolayers on surfaces of copper, silver, and gold have similar wettabilities. *J. Am. Chem. Soc.* 114:1990–1995.

Lal, R., and S. A. John. 1994. Biological applications of atomic force microscopy. *Am. J. Physiol.* 266:C1–C21.

Liu, G.-Y., and M. B. Salmeron. 1994. Reversible displacement of chemisorbed *n*-alkanethiol molecules on Au(111) surface: an atomic force microscope study. *Langmuir.* 10:367–370.

Lomant, A. J., and G. Fairbanks. 1976. Chemical probes of extended biological structures: synthesis and properties of the cleavable crosslinking reagent [^{35}S]dithio-bis(succinimidylpropionate). *J. Mol. Biol.* 104:243–261.

Lyubchenko, Y. L., P. I. Oden, D. Lampner, S. M. Lindsay, and K. A. Dunker. 1993. Atomic force microscopy of DNA and bacteriophage in air, water and propanol: the role of adhesion forces. *Nucleic Acids Res.* 21:1117–1123.

Morris, V. J. 1994. Biological applications of scanning probe microscopies. *Prog. Biophys. Mol. Biol.* 61:131–185.

Müller, D. J., G. Büldt, and A. Engel. 1995. Force-induced conformational change of bacteriorhodopsin. *J. Mol. Biol.* 249:239–243.

Nuzzo, R. G., and D. L. Allara. 1983. Adsorption of bifunctional organic disulfides on gold surfaces. *J. Am. Chem. Soc.* 105:4481–4483.

Plueddemann, E. P. 1991. Silane Coupling Agents, 2nd ed. Plenum Press, New York.

Poirier, G. E., and M. J. Tarlov. 1994. The c(4 × 2) superlattice of *n*-alkanethiol monolayers self-assembled on Au(111). *Langmuir.* 10: 2853–2856.

Porter, M. D., T. B. Bright, D. L. Allara, and C. E. D. Chidsey. 1987. Spontaneously organized molecular assemblies. 4. Structural characterization of *n*-alkylthiol monolayers on gold by optical ellipsometry, infrared spectroscopy, and electrochemistry. *J. Am. Chem. Soc.* 109: 3559–3568.

Samant, M. G., C. A. Brown, and J. G. Gordon. 1991. Structure of an ordered self-assembled monolayer of docosylmercaptan on gold(111) by surface x-ray diffraction. *Langmuir.* 7:437–439.

Schabert, F. A., and A. Engel. 1994. Reproducible acquisition of *Escherichia coli* porin surface topographs by atomic force microscopy. *Biophys. J.* 67:2394–2403.

Schaper, A., J. P. P. Starink, and T. M. Jovin. 1994. The scanning force microscopy of DNA in air and in *n*-propanol using new spreading agents. *FEBS Lett.* 355:91–95.

Sellers, H., A. Ulman, Y. Shnidman, and J. E. Eilers. 1993. Structure and binding of alkanethiolates on gold and silver surfaces: implications for self-assembled monolayers. *J. Am. Chem. Soc.* 115:9389–9401.

Shao, Z., and J. Yang. 1995. Progress in high resolution atomic force microscopy in biology. *Q. Rev. Biophys.* 28:195–251.

Sondag-Huethorst, J. A. M., C. Schönenberger, and L. G. J. Fokkink. 1994. Formation of holes in alkanethiol monolayers on gold. *J. Phys. Chem.* 98:6826–6834.

Sprik, M., E. Delamarche, B. Michel, U. Röthlisberger, M. L. Klein, H. Wolf, and H. Ringsdorf. 1994. Structure of hydrophilic self-assembled monolayers: a combined scanning tunneling microscopy and computer simulation study. *Langmuir.* 10:4116–4130.

Staros, J. V. 1988. Membrane-impermeant cross-linking reagents: probes of the structure and dynamics of membrane proteins. *Account Chem. Res.* 21:435–441.

Strong, L., and G. M. Whitesides. 1988. Structures of self-assembled monolayer films of organosulfur compounds adsorbed on gold single crystals: electron diffraction studies. *Langmuir.* 4:546–558.

Thundat, T., D. P. Allison, R. J. Warmack, G. M. Brown, K. B. Jacobson, J. J. Schrick, and T. L. Ferrell. 1992. Atomic force microscopy of DNA on mica and chemically modified mica. *Scanning Microsc.* 6:911–918.

Troughton, E. B., C. D. Bain, G. M. Whitesides, R. G. Nuzzo, D. L. Allara, and M. D. Porter. 1988. Monolayer films prepared by the spontaneous self-assembly of symmetrical and unsymmetrical dialkylsulfides from solution onto gold substrates: structure, properties, and reactivity of constituent functional groups. *Langmuir.* 4:365–385.

Tyllianakis, P. E., S. E. Kakabakos, G. P. Evangelatos, and D. S. Ithakissios. 1994. Direct colorimetric determination of solid-supported functional groups and ligands using bicinchoninic acid. *Anal. Biochem.* 219:335–340.

Vesenka, J., S. Manne, G. Yang, C. Bustamante, and E. Henderson. 1993. Humidity effects on atomic force microscopy of gold-labeled DNA on mica. *Scanning Microsc.* 7:781–788.

Wagner, P., M. Hegner, H.-J. Güntherodt, and G. Semenza. 1995. Formation and in-situ modification of monolayers chemisorbed on ultraflat template-stripped gold surfaces. *Langmuir.* 11:3867–3875.

Wagner, P., P. Kernen, M. Hegner, E. Ungewickell, and G. Semenza. 1994. Covalent anchoring of proteins onto gold-directed NHS-terminated self-assembled monolayers in aqueous buffers: SFM imaging of clathrin and its cages. *FEBS Lett.* 356:267–271.

Whitesides, G. M., and P. E. Laibinis. 1990. Wet chemical approaches to the characterization of organic surfaces: self-assembled monolayers, wetting, and the physical-organic chemistry of the solid-liquid interface. *Langmuir.* 6:87–96.

Widrig, C. A., C. Chung, and M. D. Porter. 1991. The electrochemical desorption of *n*-alkanethiol monolayers from polycrystalline Au and Ag electrodes. *J. Electroanal. Chem.* 310:335–359.

Yang, J., J. Mou, and Z. Shao. 1994a. Structure and stability of pertussis toxin studied by in situ atomic force microscopy. *FEBS Lett.* 338:89–92.

Yang, J., J. Mou, and Z. Shao. 1994b. Molecular resolution atomic force microscopy of soluble proteins in solution. *Biochim. Biophys. Acta.* 1199:105–114.

Yang, J., L. K. Tamm, A. P. Somlyo, and Z. Shao. 1993a. Promises and problems of biological atomic force microscopy. *J. Microsc.* 171: 183–198.

Yang, J., L. K. Tamm, T. W. Tillack, and Z. Shao. 1993b. New approach for atomic force microscopy of membrane proteins—the imaging of cholera toxin. *J. Mol. Biol.* 229:286–290.